JOURNAL OF THERMOPHYSICS AND HEAT TRANSFER
Vol. 8, No. 2, April–June 1994

One-Dimensional Ablation Using Landau Transformation and Finite Control Volume Procedure

B. F. Blackwell* and R. E. Hogan†
Sandia National Laboratories, Albuquerque, New Mexico 87185

A technique utilizing the Landau transformation has been developed to solve one-dimensional variable area ablation problems. It is based on applying the integral form of the conservation equations to control volumes that are moving with velocities consistent with the Landau transformation. Exponential temperature profiles are assumed to evaluate the conduction and convection fluxes at control volume faces. The technique has been applied to one-dimensional planar and cylindrical geometries with sample calculations presented to verify the accuracy of the method.

Nomenclature

A = area
C_h = aerodynamic heating transfer coefficient
C_p, C_v = specific heat at constant pressure and volume
$\dot{E}$ = energy flow rate
e = internal energy
f = see Eq. (18)
g = see Eq. (15)
i = enthalpy
i_r = freestream recovery enthalpy for aerodynamic heating boundaries
i_w = gas enthalpy at the wall temperature for aerodynamic heating boundaries
k = thermal conductivity
L = thickness of slab
$\dot{m}_c''$ = mass loss rate per unit area
Pe = Peclet no., see Eq. (16)
$\dot{q}''$ = heat flux
$\dot{\mathbf{q}}''$ = heat flux vector
$\dot{Q}$ = heat transfer rate
Q^* = heat of ablation
R_o = cylinder outer radius
r = radial coordinate
s = surface recession
$\dot{s}$ = surface recession rate
T = temperature
T_f = ablation temperature
T_0 = initial temperature
t = time
$\mathcal{V}$ = volume
V_b = velocity of control volume boundary
x = $z - s$, coordinate attached to receding surface, Fig. 1
z = coordinate attached to original surface location, Fig. 1
α = thermal diffusivity
Δr_i = $r_i - r_{i+1} > 0$
$\Delta x_{(e)}$ = $x_{i+1} - x_i > 0$
$\Delta \eta_i$ = $\eta_i - \eta_{i+1} > 0$
ε = surface emittance
η = $(L - z)/(L - s)$, Landau coordinate, Eq. (1)
ρ = density
σ = Stefan-Boltzmann constant

Subscripts
e, $e+1$, . . = indices referring to elements
i = node no.

Superscripts
m = exponent in area variation
$n+1$ = refers to current time step
$+$ = evaluated at right face of control volume
$-$ = evaluated at left face of control volume

I. Introduction

A COMMON approach to solving one-dimensional ablation problems is to attach the grid to the receding surface. This constrains all nodes wholly contained in the ablator to move with the velocity of the receding surface. The CMA code resulting from the work of Moyer and Rindal[1] utilized this approach in conjunction with upwind differencing for the apparent convection terms resulting from the translating control volumes. Blackwell[2] extended the translating grid concept using the finite control volume procedure in conjunction with the exponential differencing scheme of Spalding[3] for the convective terms. Although the translating grid scheme works quite well for one-dimensional geometries, there does not appear to be a simple way to extend the technique to multidimensional geometries. The work presented here is motivated by the desire to develop more general moving mesh techniques that can be utilized with control volume/element based methods (e.g., Blackwell and Hogan[4]) to predict ablation/shape change of and heat conduction within complex three-dimensional objects.

II. Landau Transformation

The Landau[5] transformation was originally developed for phase change problems with one-dimensional planar geometries, but will be extended here to axisymmetric geometries. It transforms the spatial coordinate such that the remaining thickness of the ablation material is always unity and is shown schematically in Fig. 1. Ablation is assumed to take place at the left boundary with recession being from left to right. The origin of the z-coordinate system is fixed in space at the original position of the ablating surface; the x-coordinate system is attached to the ablating surface; the r-coordinate system is attached to the axis of symmetry. Each of these coordinate systems has certain advantages which will become apparent in the material that follows. The current position of the surface

Received April 2, 1993; revision received July 28, 1993; accepted for publication July 29, 1993.

*Distinguished Member of Technical Staff, Thermophysics Department 1553. Member AIAA.
†Senior Member of Technical Staff, Thermal and Fluid Engineering Department 1513.

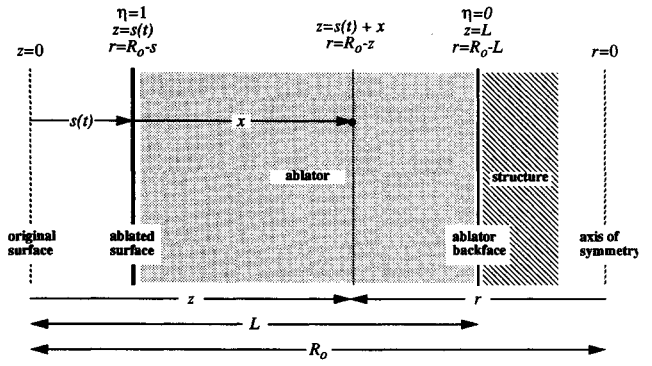

Fig. 1 Schematic of Landau transformation for one-dimensional axisymmetric geometries.

is a distance $s(t)$ to the right of the original surface location. Mathematically, the Landau[5] transformation is given by

$$\eta = \frac{L - z}{L - s}; \quad z = \eta s + (1 - \eta)L = L - \eta(L - s) \tag{1}$$

At $z = s$, $\eta = 1$; at $z = L$, $\eta = 0$. For axisymmetric geometries, the z- and r-coordinate systems are related through

$$r = R_o - z; \qquad z = R_o - r \tag{2}$$

The η and r coordinates are then related through

$$\eta = \frac{r - R_o + L}{L - s}; \qquad r = R_o - L + \eta(L - s) \tag{3}$$

We will now present the conduction equation and transform it according to Eq. (3). The one-dimensional conduction equation for arbitrary axisymmetric geometry is

$$\rho C_p \frac{\partial T}{\partial t} = \frac{1}{r^m}\frac{\partial}{\partial r}\left(kr^m \frac{\partial T}{\partial r}\right) \begin{cases} m = 0, \text{ planar} \\ m = 1, \text{ cylindrical} \\ m = 2, \text{ spherical} \end{cases} \tag{4}$$

Utilizing the chain rule and Eq. (3), the conduction equation can be transformed to

$$\rho C_p \left(\frac{\partial T}{\partial t} + \frac{\eta \dot{s}}{L - s}\frac{\partial T}{\partial \eta}\right) = \frac{1}{[R_o - L + \eta(L - s)]^m}\frac{1}{(L - s)^2}\frac{\partial}{\partial \eta} \times \left\{k[R_o - L + \eta(L - s)]^m \frac{\partial T}{\partial \eta}\right\} \tag{5}$$

Although there is no intent to use Eq. (5) in either a finite difference or finite element algorithm, some insight can be gained by examining this equation. First, Eq. (5) has a convection-like term that is not present in Eq. (4); this additional term is physically due to the grid motion. Second, the velocity of any line of η = constant is $\eta\dot{s}$, and it is the coefficient of the spatial derivative on the left side of Eq. (5). This can be seen by differentiating Eq. (1) with respect to time while holding η constant, resulting in the velocity V_b of any η = constant line:

$$V_b(\eta, t) = \left(\frac{\partial z}{\partial t}\right)_\eta = \eta\dot{s}; \quad V_b(1, t) = \dot{s}; \quad V_b(0, t) = 0 \tag{6}$$

The outer surface of the ablator ($\eta = 1$) moves with a velocity $\dot{s}$, the back face of the ablator ($\eta = 0$) moves with a velocity of zero, and intermediate points have a velocity of $\eta\dot{s}$.

Coordinate transformations similar in concept (but different in form) to that discussed above have been utilized by Popper and Toong,[6] Rafinejad and Kendall,[7] King et al.,[8] Cai and Hou,[9] and Muramoto et al.[10] In each of these references, the transformed partial differential equation was then solved using finite difference techniques. A completely different approach using the "enthalpy method" was presented by Hunter and Kuttler.[11] In the sections that follow, a technique will be presented that allows one to go directly from the integral form of the energy equation for control volumes of finite size to algebraic relationships in the unknown nodal temperatures.

III. Control Volume Motion Consistent with Landau Transformation

Rather than using a finite difference or finite element method to solve Eq. (5), conservation principles will be applied directly to control volumes that move with velocities consistent with the Landau[5] transformation. Figure 2 is a schematic of a variable area control volume surrounding node i and the two elements that contribute to this control volume. Control volume faces are located midway between node points; therefore the right and left control volume faces are moving at velocities of $\dot{s}(\eta_i - \Delta\eta_i/2)$ and $\dot{s}(\eta_i + \Delta\eta_{i-1}/2)$, respectively. The integral form of the conservation principles will now be applied to these moving control volumes. The point of view will be that of an observer moving with the control volume. Material will be convected into and out of the control volume due to the control volume motion.

IV. Geometric Conservation Law

Thomas and Lombard[12] introduced the concept of the geometric conservation law and applied it to flow computations on moving grids. This concept requires that the mesh satisfy a "continuity-like" requirement. For the problems under consideration here, the geometric conservation law is

$$-\iint_A V_b \cdot dA + \frac{d}{dt}\iiint_{\mathcal{V}} d\mathcal{V} = 0 \tag{7}$$

where V_b is the velocity of the control volume boundary, and A and $\mathcal{V}$ are control volume area and volume, respectively. This equation is essentially the continuity equation for a constant density medium. Application of Eq. (7) to the one-dimensional moving control volume shown in Fig. 2 yields

$$AV_b|_{x_i^-} - AV_b|_{x_i^+} + \frac{d}{dt}\int_{x_i - x_i^+} d\mathcal{V} + \frac{d}{dt}\int_{x_i^- - x_i} d\mathcal{V} = 0 \tag{8}$$

For an arbitrary one-dimensional axisymmetric geometry, the area variation with radial position is

$$A(r) = 2m\pi r^m \tag{9}$$

and the volume of the portion of the control volume on each side of node i is

$$\mathcal{V}_i^- = \frac{2m\pi}{m + 1}\left[\left(r_i + \frac{\Delta r_{i-1}}{2}\right)^{m+1} - r_i^{m+1}\right]$$
$$\mathcal{V}_i^+ = \frac{2m\pi}{m + 1}\left[r_i^{m+1} - \left(r_i - \frac{\Delta r_i}{2}\right)^{m+1}\right] \tag{10}$$

Utilizing Eqs. (9) and (10), one can demonstrate that the proposed grid motion scheme identically satisfies the geo-

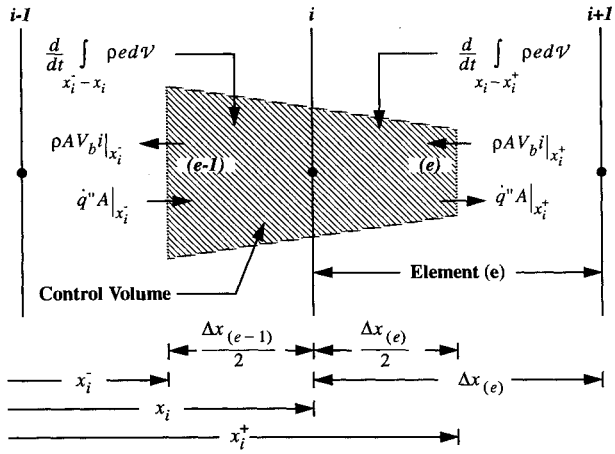

Fig. 2 Schematic of control volume surrounding node i and the two elements (e) and (e-1) that form it.

metric conservation law, Eq. (8), for arbitrary one-dimensional axisymmetric geometries.

V. Energy Conservation for Moving Control Volumes

Instead of working with the transformed Eq. (5), there are some advantages to working directly with the integral form of the energy equation. For heat conduction in a solid without sources and in which the control volume boundary surfaces are moving with velocity V_b, the energy equation can be written as

$$\iint_A \dot{q}''\cdot dA - \iint_A \rho i V_b \cdot dA + \frac{d}{dt}\iiint_{\mathcal{V}} \rho e \, d\mathcal{V} = 0 \quad (11)$$

where $\dot{q}''$ is the conduction heat flux vector, $\rho i V_b$ is the enthalpy flux crossing the control volume boundary due to control surface motion, ρe is the internal energy per unit volume, and A and $\mathcal{V}$ are surface area and volume of the control volume, respectively. We will use the one-dimensional analog of Eq. (11) and develop equations in terms of nodal temperatures. Figure 2 is a schematic of the two elements (e-1) and (e) that contribute to the energy balance on node i; note that the area is assumed to be a function of position. The one-dimensional equivalent to Eq. (11) is

$$\dot{q}''A|_{x_i^+} - \dot{q}''A|_{x_i^-} + \rho A V_b i|_{x_i^-} - \rho A V_b i|_{x_i^+} + \frac{d}{dt}\int_{x_i - x_i^+} \rho e \, d\mathcal{V} + \frac{d}{dt}\int_{x_i^- - x_i} \rho e \, d\mathcal{V} = 0 \quad (12)$$

In order to evaluate the heat and energy flux terms crossing the control volume boundary, it is necessary to make some assumptions about how the temperature varies within an element; this will be addressed in the next section.

VI. Element Temperature Profile

The element temperature profile is assumed to be exponential in form. This technique was first proposed by Spalding[3] for solving convection problems, and has been implemented by Blackwell[2] for one-dimensional ablation problems. A brief summary of the approach will be presented here. The concept is based on the fact that the analytical solution for the steady-state temperature profile of a semi-infinite one-dimensional planar body ablating at a fixed temperature (T_f) is exponential in form, and is given by

$$\frac{T(x) - T_0}{T_f - T_0} = \exp\left(-\frac{\dot{s}x}{\alpha}\right) \quad (13)$$

Note that the x coordinate is measured from the instantaneous ablated surface location (see Fig. 1 for details). For control volume boundaries located at the midpoint of the elements, it can be shown that the temperature at the control volume face is a weighted average of the two nodal temperatures

$$T[x_i + \Delta x_{(e)}] = g_{(e)}T_i + [1 - g_{(e)}]T_{i+1} \quad (14)$$

where

$$g_{(e)} = \frac{\exp[Pe_{(e)}/2] - 1}{\exp[Pe_{(e)}] - 1} \quad (15)$$

$$Pe_{(e)} = \frac{\dot{s}\Delta x_{(e)}}{\alpha_{(e)}} \quad (16)$$

For grid scale Peclet number approaching zero, $g_{(e)} = 0.5$ (central differencing); for $Pe_{(e)} > 10$, $g_{(e)}$ becomes quite small (upwind differencing).

The conduction heat flux crossing the control volume boundary can also be found from the element temperature profile and is as follows:

$$\dot{q}''(x_i + \Delta x_{(e)}/2) = -k\left.\frac{dT}{dx}\right|_{x_i + \Delta x_{(e)}/2} = -f_{(e)}k\frac{T_{i+1} - T_i}{\Delta x_{(e)}} \quad (17)$$

where

$$f_{(e)} = \frac{Pe_{(e)}\exp[Pe_{(e)}/2]}{\exp[Pe_{(e)}] - 1} \quad (18)$$

At zero grid scale Peclet number, $f_{(e)} = 1$ (central differencing); for $Pe_{(e)}$ large, $f_{(e)}$ becomes small (upwind differencing). Equations (14) and (17) allow a continuous transition from central differencing for zero grid scale Peclet number to upwind differencing for large grid scale Peclet number. Additional details on the development of the above relationships can be found in Blackwell.[2]

VII. Development of Element Matrices

Element matrices will be developed for the conduction, convection, and storage terms in the energy equation. Even though control volume based methods are being used, the development of element matrices will allow the global equations to be assembled from the element matrices as in the finite element method.

A. Conduction

Equation (17) gives the heat flux across a control volume face. Using this result, the element conduction matrix can be written as

$$\begin{bmatrix} \dot{Q}_i \\ \dot{Q}_{i+1} \end{bmatrix}_{(e)} = \left(\frac{kA}{\Delta x}\right)_{(e)} f_{(e)} \begin{bmatrix} 1 & -1 \\ -1 & 1 \end{bmatrix} \begin{bmatrix} T_i \\ T_{i+1} \end{bmatrix} \quad (19)$$

where

$$\Delta x_{(e)} = (L - s)\Delta\eta_{(e)} \quad (20)$$

Once the η mesh is established, it is independent of time. However, the x mesh is continuously changing with time and is recomputed from Eq. (20) at each time step.

B. Convection

Equation (14) is the recipe that will be used to interpolate within an element to determine the temperature at the control volume face. If i is replaced with C_pT, the element convection matrix can be written as

$$\begin{bmatrix} \dot{E}_i \\ \dot{E}_{i+1} \end{bmatrix} = (\rho V_b A C_p)_{(e)} \begin{bmatrix} -g & -(1-g) \\ g & (1-g) \end{bmatrix} \begin{bmatrix} T_i \\ T_{i+1} \end{bmatrix} \tag{21}$$

where the velocity of the control volume is given by

$$V_{b_{(e)}} = \dot{s}(\eta_i - \Delta\eta_i/2) \tag{22}$$

C. Storage/Volume Change

In Eq. (12), e will be replaced by C_vT. (Care must be exercised to insure that the internal energy reference condition is consistent with that used in the surface energy balance enthalpy terms.) The energy content arising from the contribution of element "e" to the energy balance on control volume "i" can be written as

$$\frac{\mathrm{d}}{\mathrm{d}t}\int_{x_i - x_i^+} \rho e \, \mathrm{d}\mathcal{V} \approx (\rho C_v)_{(e)} \frac{\mathrm{d}}{\mathrm{d}t}\int_{x_i}^{x_i^+} T(x) \, \mathrm{d}\mathcal{V} \tag{23}$$

where the element volumetric heat capacity is assumed to be independent of position and time (for at least one time step). To be completely consistent, one should use the exponential element temperature profile and the area variation with position to evaluate the integral on the right side of Eq. (23). Instead, some approximations will be introduced. The above integral will be approximated as follows:

$$\int_{x_i}^{x_i^+} T(x) \, \mathrm{d}\mathcal{V} \approx \frac{\mathcal{V}_{(e)}}{2}\left(\frac{3}{4}T_i + \frac{1}{4}T_{i+1}\right) \tag{24}$$

Equation (24) is consistent with using an effective volume $\mathcal{V}_{(e)}/2$ and a linear element temperature profile. Equation (24) can be differentiated with respect to time to yield the combined storage/volume change term

$$\frac{\mathrm{d}}{\mathrm{d}t}\int_{x_i - x_i^+} \rho e \, \mathrm{d}\mathcal{V} \approx (\rho C_v)_{(e)}\left[\frac{\mathcal{V}_{(e)}}{2}\frac{\mathrm{d}}{\mathrm{d}t}\left(\frac{3}{4}T_i + \frac{1}{4}T_{i+1}\right) + \left(\frac{3}{4}T_i + \frac{1}{4}T_{i+1}\right)\frac{1}{2}\frac{\mathrm{d}\mathcal{V}_{(e)}}{\mathrm{d}t}\right] \tag{25}$$

The element volume is

$$\mathcal{V}_{(e)} = \frac{2m\pi}{m+1}(r_i^{m+1} - r_{i+1}^{m+1}) \tag{26}$$

and its time derivative is

$$\frac{\mathrm{d}\mathcal{V}_{(e)}}{\mathrm{d}t} = -\dot{s}(A_i\eta_i - A_{i+1}\eta_{i+1}) \tag{27}$$

where A_i is the nodal area and can be evaluated from Eq. (9).

The element storage/volume change matrix can now be written as

$$(\rho C_v)_{(e)}\frac{\mathcal{V}_{(e)}}{2}\begin{bmatrix} \frac{3}{4} & \frac{1}{4} \\ \frac{1}{4} & \frac{3}{4} \end{bmatrix}\frac{\mathrm{d}}{\mathrm{d}t}\begin{bmatrix} T_i \\ T_{i+1} \end{bmatrix} + (\rho C_v)_{(e)}\frac{1}{2}\frac{\mathrm{d}\mathcal{V}_{(e)}}{\mathrm{d}t}\begin{bmatrix} \frac{3}{4} & \frac{1}{4} \\ \frac{1}{4} & \frac{3}{4} \end{bmatrix}\begin{bmatrix} T_i \\ T_{i+1} \end{bmatrix} \tag{28}$$

A common simplification for Eq. (28) is the lumped capacitance approach in which $\frac{3}{4} \to 1$ and $\frac{1}{4} \to 0$. If a Galerkin finite element approach had been used, then $\frac{3}{4} \to \frac{2}{3}$ and $\frac{1}{4} \to \frac{1}{3}$.

Up to this point, the time integration scheme has not been specified. For the results to be presented in this article, the fully implicit time integration scheme and lumped capacitance approximation were used. The usual element assembly rules can be applied to form the global temperature matrix.

VIII. Boundary Conditions

The computer code that has evolved from this work will handle a general boundary condition of the form

$$-k\left.\frac{\partial T}{\partial x}\right|_{x=0} = C_h(i_r - i_w) + \alpha_w\dot{q}_r'' - \varepsilon_w\sigma(T_w^4 - T_\infty^4) - \dot{m}_c''(i_w - i_c) \tag{29}$$

where C_h is an aerodynamic heating heat transfer coefficient based on enthalpy difference driving potential, $\dot{q}_r''$ is an input radiation heat flux, and $\dot{m}_c''$ is the mass flux which may be a complex function of surface temperature and pressure. For the calculations presented here, a simplified "heat of ablation" model will be used in which ablation takes place at a fixed surface temperature. This boundary condition is given as

$$-k\left.\frac{\partial T}{\partial x}\right|_{x=0} = \dot{q}'' - \dot{m}_c''Q^* \tag{30}$$

where $\dot{q}''$ is a specified input heat flux and Q^* is the heat of ablation (energy per unit mass consumed in the ablation process).

IX. Example Calculations

A. Planar Geometry, Steady State

In order to verify the accuracy of this method, an example problem consisting of a planar slab with a specified (constant) heat flux was considered. The geometry, material properties, and boundary conditions are given in Fig. 3. The recession rate at steady state was computed using the analytical solution, Eq. (13), and the boundary condition, Eq. (30). The purpose of this example problem is to demonstrate the accuracy of the steady-state surface recession rate predictions and the rate of convergence as the mesh is refined. If this example problem is started from a uniform initial temperature, some finite amount of time is required to reach a steady state. Instead of using a uniform initial temperature, the exact profile given by Eq. (13) was used. A nonuniform mesh based on the requirement that the ratio of the thickness between adjacent elements follow a geometric progression was used. Details of this mesh generator are given in Blackwell et al.[13] The user specifies the thickness of the element at the ablating surface and the total number of elements; the code determines the distribution of element thicknesses that is consistent with the total thickness constraint. The mesh was refined by doubling the total number of elements and cutting the first element thickness in half; the time step was adjusted such that $\alpha\Delta t\Delta x_1^2 =$

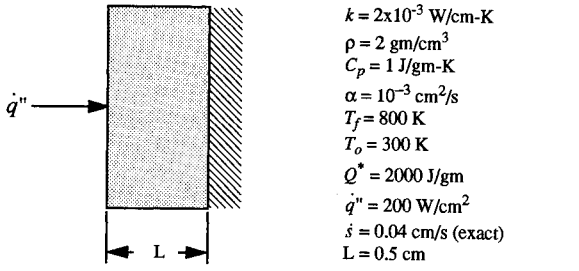

Fig. 3 Example problem with steady-state ablation of a planar slab.

10 for all cases considered. The results of these calculations are summarized in Table 1 and Fig. 4. For the coarsest mesh, the error in surface recession is a respectable 0.02%. As the mesh was refined, the recession rate error decreases approximately quadratically with the number of elements.

In addition to surface recession rate errors, the error in the steady-state temperature profile at 2 s was also computed and is shown in Fig. 5. At the front face, the errors are identically zero because of the specified temperature boundary condition. The maximum temperature error occurs in the neighborhood of $x = 0.07$ cm for all three meshes considered. For the 10 element case, the mesh near the back face may be somewhat coarse. As the mesh is refined, the peaks in the temperature error decrease. The temperature profile is predicted with good accuracy.

B. Cylindrical Geometry, Transient Ablation

The cylindrical geometry example problem is the same as the planar geometry problem described in Fig. 3 with the exception that the radius $R_o = L$. Unfortunately, for a finite radius cylinder, there is not an analogous steady-state solution. Consequently, Richardson's extrapolation to the limit will be used to estimate the surface recession rate at 2 s for an infinite number of elements. For quadratic convergence (we do not know that the convergence is quadratic; however, it should be a reasonable approximation based on the results for the planar geometry example), in the mesh spacing, the extrapolation relationship used was

$$\dot{s}(\Delta x = 0) = [4\dot{s}(\Delta x/2) - \dot{s}(\Delta x)]/3 \tag{31}$$

For this series of calculations, the initial temperature profile was the exponential profile given by Eq. (12). The results are summarized in Table 2 and Fig. 4. It appears that as the mesh is refined, the recession rate error decreases approximately quadratically in the number of elements. The results for 80 elements were not plotted because of inadequate significant digits in the calculations.

Table 1 Planar geometry-parameters for mesh refinement study and predicted recession rate at 2 s; $\alpha\Delta t/\Delta x_1^2 = 10$ for all cases

No. Δx	Δx_1, cm	Δt, s	$\dot{s}$ @ 2 s	% Error
10	0.001	0.01	0.0400087	0.02175
20	0.0005	0.0025	0.0400020	0.00500
40	0.00025	0.000625	0.0400005	0.00125

Table 2 Cylindrical geometry-parameters for mesh refinement study and predicted recession rate at 2 s; $\alpha\Delta t/\Delta x_1^2 = 10$ for all cases

No. Δx	Δx_1, cm	Δt, s	$\dot{s}$ @ 2 s	% Error
10	0.001	0.01	0.0408370	0.0890
20	0.0005	0.0025	0.0408094	0.0214
40	0.00025	0.000625	0.0408028	0.0052
80	0.000125	0.00015625	0.0408012	——
∞	0	——	0.04080067	——

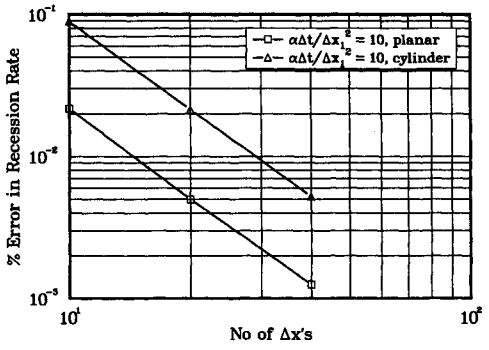

Fig. 4 % Error in recession rate at 2 s as mesh is refined; $\alpha\Delta t/\Delta x_1^2 = 10$ for all cases.

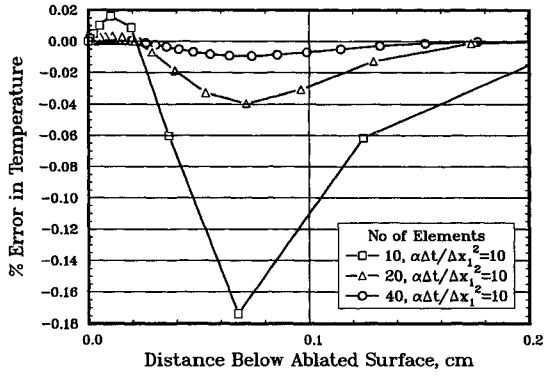

Fig. 5 % Error in temperature at 2 s as mesh is refined; $\alpha\Delta t/\Delta x_1^2 = 10$ for all cases.

X. Summary

A general algorithm for solving one-dimensional variable area ablation problems has been developed. It is based on the Landau[5] transformation. However, its implementation is not through the formal transformation of the governing partial differential equation, but through a novel application of the integral form of the conservation equations on control volumes that move in a manner consistent with the Landau transformation. The relative element size remains fixed while the computational domain is shrinking due to ablation. This approach has the advantage of allowing one to concentrate elements near the heated surface and have them remain there throughout the problem time.

Exponential element temperature profiles were used to evaluate conduction and convection due to the moving mesh. Element matrices were presented for conduction, convection, and storage/volume change.

Sample calculations were performed for a planar body for which an analytical solution exists for the steady-state ablation rate and temperature profile. The agreement was excellent and approximate quadratic convergence was achieved as the mesh was refined. Calculations were also performed for a cylindrical body, and Richardson's extrapolation to the limit was used to estimate the recession rate for an infinite number of elements. Again, the agreement was excellent with approximately quadratic convergence. Although not demonstrated in this article, the moving/contracting mesh has been coupled to a stationary mesh for backup materials and has been utilized to solve a variety of practical real world ablation problems including graphite ablation at a nonconstant temperature.

Preliminary work to extend some of the above concepts to two-dimensional axisymmetric geometries using a "motion along spines" algorithm has been presented in Ref. 14. Conceptually, it appears that these techniques can be extended to variable density problems such as charring ablators.

Acknowledgments

This work was performed at Sandia National Laboratories, Albuquerque, New Mexico, and was supported by the U.S. Department of Energy under Contract DE-AC04-76DP00789.

References

[1]Moyer, C. B., and Rindal, R. A., "An Analysis of the Coupled Chemically Reacting Boundary Layer and Charring Ablator, Part II, Finite Difference Solution for the In-Depth Response of Charring Materials Considering Surface Chemical and Energy Balances," NASA CR-1061, June 1968.

[2]Blackwell, B. F., "Numerical Prediction of One-Dimensional Ablation Using a Finite Control Volume Procedure with Exponential Differencing," *Numerical Heat Transfer*, Vol. 14, No. 1, 1988, pp. 17–34.

[3]Spalding, D. B., "A Novel Finite-Difference Formulation for Differential Expressions Involving Both First and Second Derivatives," *International Journal for Numerical Methods in Engineering*, Vol. 4, No. 4, 1972, pp. 551–559.

[4]Blackwell, B. F., and Hogan, R. E., "Numerical Solution of Axisymmetric Heat Conduction Problems Using Finite Control Volume Technique," *Journal of Thermophysics and Heat Transfer*, Vol. 7, No. 3, 1993, pp. 462–471; see also AIAA Paper 91-1353, June 1991.

[5]Landau, H. G., "Heat Conduction in a Melting Solid," *Quarterly of Applied Math*, Vol. VIII, No. 1, 1950, pp. 81–94.

[6]Popper, L. A., and Toong, T. Y., "Three-Dimensional Ablation Considering Shape Changes and Internal Heat Conduction," AIAA Paper 70-199, Jan. 1970.

[7]Rafinejad, D., and Kendall, R. M., "Transient Conduction and Shape Change Calculation of Three-Dimensional Nose Tips," AIAA Paper 76-168, Jan. 1976.

[8]King, H. H. C., Muramoto, K. K., Murray, A. L., and Pronchick, S. W., "ABRES Shape Change Code (ASCC 86), Technical Report and User's Manual," BMO TR-87-57, Headquarters Ballistic Missile Office/MYES, Norton AFB, CA, Dec. 1986.

[9]Cai, T., and Hou, X., "A Simple Method for Tackling Moving Boundary in Numerical Simulation of Temperature Response of the Solid Rocket Motor," AIAA Paper 88-0083, Jan. 1988.

[10]Muramoto, K. K., Squire, T. H., and Thompson, C. F., Jr., "A Thermal Analysis Code for Three-Dimensional Wing Leading Edges," AIAA Paper 91-1354, June 1991.

[11]Hunter, L. W., and Kuttler, J. R., "Enthalpy Method for Ablation-Type Moving Boundary Problems," *Journal of Thermophysics and Heat Transfer*, Vol. 5, No. 2, 1991, pp. 240–242.

[12]Thomas, P. D., and Lombard, C. K., "Geometric Conservation Law and Its Application to Flow Computations on Moving Grids," *AIAA Journal*, Vol. 17, No. 10, 1979, pp. 1030–1037.

[13]Blackwell, B. F., Douglass, R. W., and Wolf, H., "A User's Manual for the Sandia One-Dimensional Direct and Inverse Thermal (SODDIT) Code," SAND85-2478, Sandia National Lab., Albuquerque, NM, May 1987.

[14]Blackwell, B. F., Thornton, A. L., and Hogan, R. E., "Ablation Problems Using a Finite Control Volume Technique," *Computational Modelling of Free and Moving Boundary Problems II*, Computational Mechanics Publications, Southampton, England, UK, 1993, pp. 295–302.